

Clusters and halos in light nuclei

Thomas Neff

GSI Helmholtzzentrum für Schwerionenforschung GmbH, Planckstraße 1, 64291 Darmstadt, Germany

E-mail: t.neff@gsi.de

Abstract. The fermionic molecular dynamics approach uses Gaussian wave packets as single-particle basis states. Many-body basis states are Slater determinants projected on parity, angular momentum and total linear momentum. The wave-packet basis is very flexible – FMD contains harmonic oscillator shell model and Brink-type cluster states as special cases. The parameters of the wave packets are obtained by variation. A realistic effective interaction derived from the Argonne V18 interaction by means of the unitary correlation operator method is employed. We discuss the fully microscopic calculation of the ${}^3\text{He}(\alpha, \gamma){}^7\text{Be}$ capture reaction within the FMD approach. The model space contains frozen cluster configurations at large distances and polarized configurations in the interaction region. The polarized configurations are essential for a successful description of the ${}^7\text{Be}$ bound state properties and for the S - and D -wave scattering states. The calculated cross section agrees well with recent measurements regarding both the absolute normalization and the energy dependence. We also discuss the structure of the cluster states, including the famous Hoyle state, in ${}^{12}\text{C}$. From the two-body densities we conclude that the Hoyle state has a spatially extended triangular α -cluster structure, whereas the third 0^+ state features a chain-like obtuse triangle structure. We also calculate the $N\hbar\Omega$ decomposition of our wave functions to illuminate the challenges of no-core shell model calculations for these cluster states.

1. Introduction

Cluster and halo states present a challenge for nuclear structure calculations. They are typically found close to thresholds and feature extended tails in the wave functions. In many-body approaches like the no-core shell model where the wave functions are expanded in a harmonic oscillator basis the description of such spatially extended wave functions require huge model spaces. Cluster models on the other hand are by construction well suited to describe the asymptotics of such states. However cluster models are an oversimplification. With realistic interactions it is not possible to obtain reasonable results as polarization effects of the clusters are missing. With the fermionic molecular dynamics approach we attempt to combine the advantages of a microscopic model with those of the cluster model.

2. Fermionic Molecular Dynamics

In the fermionic molecular dynamics (FMD) approach we employ Gaussian wave packets

$$\langle \mathbf{x} | q \rangle = \frac{(\mathbf{x} - \mathbf{b})^2}{2a} \otimes |\chi^\uparrow, \chi^\downarrow\rangle \otimes |\xi\rangle \quad (1)$$

as single-particle basis states. The complex parameters \mathbf{b} encode the mean positions and momenta of the wave packets and a the widths of the wave packets. The spins can assume

any direction, isospin is ± 1 denoting a proton or a neutron. Intrinsic many-body basis states are Slater determinants

$$|Q\rangle = \mathcal{A} \{ |q_1\rangle \otimes \dots \otimes |q_A\rangle \}. \quad (2)$$

The intrinsic states $|Q\rangle$ reflect deformation or clustering and break the symmetries of the Hamiltonian with respect to parity, rotation and translation. To restore the symmetries the intrinsic basis states are projected on parity, angular momentum and total linear momentum

$$|Q; J^\pi MK; \mathbf{P} = 0\rangle = \hat{P}^\pi \hat{P}_{MK}^J \hat{P}^{\mathbf{P}=0} |Q\rangle. \quad (3)$$

In a full FMD calculation the many-body Hilbert space is spanned by a set of N intrinsic basis states $\{|Q^{(a)}\rangle, a = 1, \dots, N\}$. In the end the full wave many-body state is obtained by diagonalizing the Hamiltonian in this set of non-orthogonal basis states.

3. Unitary Correlation Operator Method

Starting from the realistic Argonne V18 interaction [1] we derive an effective low-momentum interaction using the unitary correlation operator method (UCOM). The basic idea of the UCOM approach is to explicitly include short-range central and tensor correlations into the many-body state by means of a unitary operator [2, 3, 4]. The correlation operators can also be mapped onto the Hamiltonian to define a correlated interaction which not only contains two-body but also higher order contributions. However, the UCOM interaction is defined as the two-body part of the correlated Hamiltonian and we neglect higher order terms. The UCOM interaction provides the same phase shifts as the original interaction but behaves differently in many-body systems. No-core shell model calculations show that the two-body UCOM interaction gives a good description of s - and light p -shell nuclei [4].

4. Radiative capture reaction ${}^3\text{He}(\alpha, \gamma){}^7\text{Be}$

A recent application of the FMD approach is the calculation of the ${}^3\text{He}(\alpha, \gamma){}^7\text{Be}$ radiative capture reaction [5]. This reaction plays an important role in the solar proton-proton chains and determines the production of ${}^7\text{Be}$ and ${}^8\text{B}$ neutrinos [6, 7]. This reaction has been studied extensively from the experimental side in recent years [8, 9, 10, 11, 12]. However it is still not possible to reach the low energies relevant for solar burning in experiment. From the theory side this reaction has been investigated using simple potential models, where ${}^3\text{He}$ and ${}^4\text{He}$ are treated as point-like particles interacting via an effective nucleus-nucleus potential, e.g., [13] or microscopic cluster models, e.g., [14, 15] where the ${}^7\text{Be}$ bound and scattering states are constructed from microscopic ${}^3\text{He}$ and ${}^4\text{He}$ clusters interacting via an effective nucleon-nucleon interaction. *Ab-initio* calculations using variational Monte Carlo [16] and no-core shell model wave functions [17] were used to calculate asymptotic normalization coefficients for the bound states but relied on potential models for the scattering phase shifts.

In the FMD calculation for the ${}^3\text{He}(\alpha, \gamma){}^7\text{Be}$ reaction we divide the model space into two regions. In the external region bound and scattering states are described by ${}^3\text{He}$ and ${}^4\text{He}$ clusters in their FMD ground states. These microscopic wave functions can also be rewritten as resonating group (RGM) wave functions. The RGM representation allows us to include boundary conditions for bound and scattering states by matching to Whittaker and Coulomb functions at the channel radius ($a=12$ fm). For this we employ the microscopic R -matrix method developed by the Brussels group [18]. In the interaction region the model space is enlarged by additional FMD many-body configurations obtained by variation after parity and angular momentum projection on spin-parity $1/2^+$, $3/2^+$, $5/2^+$ and $3/2^-$, $1/2^-$, $7/2^-$, $5/2^-$. A constraint on the radius of the intrinsic states is used to vary the distance between the clusters.

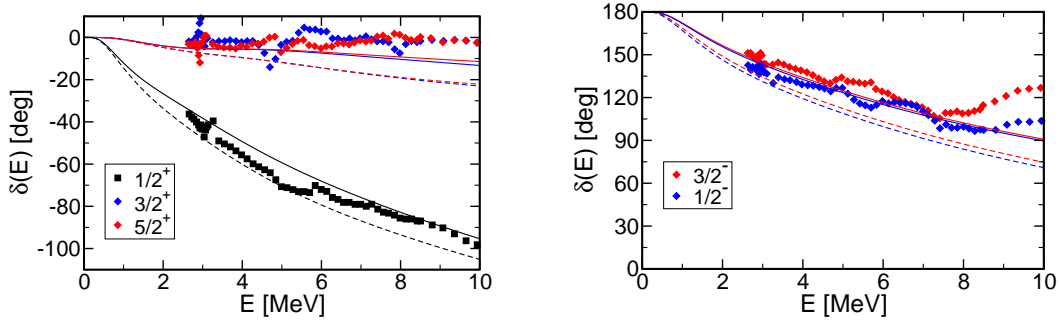


Figure 1. ^4He - ^3He scattering phase shifts. Dashed lines show results using only frozen configurations, solid lines show results with full FMD model space. Left: S - and D -wave phase shifts. Right: P -wave phase shifts. Experimental results are from [20] and [21].

4.1. Capture Cross Section

For energies up to 2.5 MeV only the capture from S - and D -wave scattering states into the $3/2^-$ and $1/2^-$ bound states has to be considered. The addition of polarized configurations is essential in the FMD framework — using the frozen configurations only, ^7Be is only bound by 200 keV. Including the polarized configurations the $3/2^-$ state is bound by 1.49 MeV and the $1/2^-$ state by 1.31 MeV with respect to the cluster threshold. The calculated splitting between the two states is too small compared to the experimental value of 430 keV. This is related to a deficiency of the two-body interaction — additional spin-orbit strength is assumed to be coming from three-body forces. Fortunately it turns out that the capture cross section depends strongly on the centroid energy, which is reproduced nicely, but only very weakly on the splitting between the two bound states. An important test of the ground state wave function is provided by the charge radius. The calculated value 2.67 fm agrees well with the experimental value of 2.647(17) fm [19]. This is important as the dipole matrix element and therefore the capture cross section depends on an accurate description of the tail of the bound state wave functions. In Fig. 1 the calculated phase shifts for the S -, D - and P -waves are compared with the experimental phase shift analyses [20, 21]. There is a noticeable change in the results going from the model space containing only the frozen configurations to the full FMD model space. In case of the S - and D -wave phase shifts we find a good agreement with the experimental data. Also the P -wave phase shifts are essentially in good agreement with experiment, with the exception of the splitting.

The capture cross section is calculated using the microscopic wave functions of the bound and scattering states. The result for the total cross section for the $^3\text{He}(\alpha, \gamma)^7\text{Be}$ capture is shown in the left part of Fig. 2 in form of the astrophysical S -factor. It agrees very well with the recent experimental data both in absolute normalization and in the energy dependence. Our result for the isospin mirror reaction $^3\text{H}(\alpha, \gamma)^7\text{Li}$ is shown on the right hand side of Fig. 2. Whereas the energy dependence of the calculated S -factor agrees very well with the data the absolute cross section is larger than the data by Brune *et al.* by about 15%. This is surprising as the FMD results for the ^7Li bound states and the scattering phase shifts are of similar quality than those for ^7Be .

The total cross section can be decomposed into S - and D -wave contributions as shown in the left part of Fig. 3. If we compare our results with microscopic cluster model calculations, for example to those by Kajino [15] we observe that the biggest differences are found in the S -wave contribution. Our results also deviate from the empirical correlation between radius or quadrupole moment of the ^7Be ground state with the S -factor at zero energy that was found in the microscopic cluster model using different phenomenological interactions.

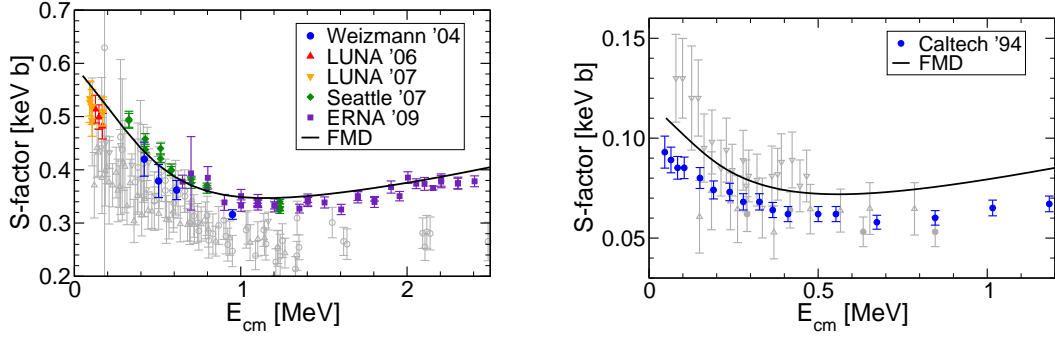


Figure 2. Left: S -factor for the ${}^3\text{He}(\alpha, \gamma){}^7\text{Be}$ reaction. Recent experimental data [8, 9, 10, 11, 12] are shown as colored symbols, older data as gray symbols. Right: S -factor for the ${}^3\text{H}(\alpha, \gamma){}^7\text{Li}$ reaction. Most recent data [22] is shown as colored symbols, older data as gray symbols.

For a comparison with the cluster model picture we can analyze the A -body bound and scattering state wave functions in terms of overlap functions. Here the full microscopic wave function is projected on the subspace of cluster configurations. If one takes antisymmetrization between the clusters into account properly (by folding with the square-root of the RGM norm kernel) these overlap functions can be interpreted as the relative wave functions of point-like ${}^3\text{He}$ and ${}^4\text{He}$ clusters. It is interesting that the overlap functions deviate from the Whittaker and Coulomb functions, that describe the asymptotic behavior of the cluster motion for bound and scattering states, up to distances of about 9 fm. These differences from the asymptotic behavior manifest themselves also in the dipole strength. The dipole matrix elements calculated from the overlap functions as shown in the right part of Fig. 3 agree with the matrix elements from the microscopic wave functions within 2%. They have sizable contributions already for distances as small as 3 fm and deviate significantly from matrix elements calculated from the asymptotic Whittaker and Coulomb functions to distances of up to 10 fm. This differences indicate that considering this reaction as a simple external capture process is not possible.

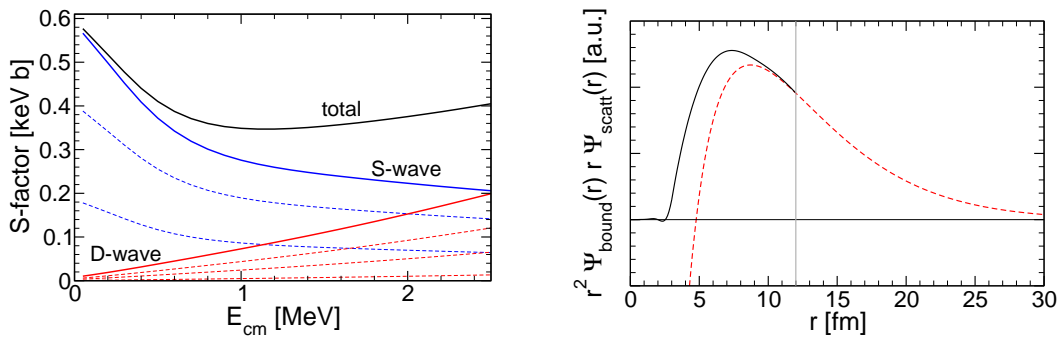


Figure 3. Left: S - and D -wave contributions to the S -factor for the ${}^3\text{He}(\alpha, \gamma){}^7\text{Be}$ reaction. Dashed lines show contributions of individual transitions. Right: Dipole strength between the $3/2^-$ bound state and the 50 keV $1/2^+$ scattering state calculated from the overlap functions (solid line), from the Whittaker and Coulomb functions matched at the channel radius (dashed line).

5. Cluster States in ^{12}C

The structure of the second 0^+ state in ^{12}C , the famous Hoyle state, is still one of the hottest topics in nuclear structure. In [23] we investigated the structure of the Hoyle state using the FMD approach. The model space consisted of configurations obtained by variation and a full set of three- α configurations. A UCOM interaction with some phenomenological modifications regarding the strength of the spin-orbit force and the saturation properties of the two-body interaction was used in that calculation. We compared the results with a microscopic cluster model using a phenomenological Volkov interaction. These cluster model calculations reproduced previous results by Kamimura [24] and are also very close to those obtained by Funaki et al. [25]. We found for both models that the Hoyle state has a very dilute, extended three- α structure. This is illustrated in Fig. 4 where we show the intrinsic FMD basis states that have the largest overlap with the ground state and the Hoyle state.

We used these wave functions also to calculate the transition form factor from the ground state to the Hoyle state. This transition form factor can be directly compared to electron scattering data [23, 26]. The good agreement of calculation and experiment is a strong confirmation for a spatially extended structure for the Hoyle state.

5.1. Two-body densities

Observables like radii and form factors are scalar quantities that provide information about the size of the states but they do not provide direct information about the structure of the states. The old question whether the Hoyle state should be interpreted as a linear chain of α -particles, a triangular structure or a gas-like structure can therefore not be answered directly by these experimental observables. There is also the question of how we should compare the wave functions obtained in different many-body approaches like the cluster model, the no-core shell model or as obtained on the lattice [27].

In case of FMD or the cluster model the individual basis states can be easily interpreted in terms of the intrinsic structure as shown in Fig. 4. However the eigenstates are linear combinations of many basis states and the non-orthogonality of the basis states might question the validity of the obtained picture.

To remedy this situation we propose to use two-body densities to analyze the structure of the ^{12}C eigenstates. In Fig. 5 we show the diagonal part of the two-body density integrated over the center-of-mass coordinates and summed over all spin-isospin channels which can be expressed as

$$\rho^{(2)}(\mathbf{r}) = \langle \Psi | \sum_{i < j} \delta(\hat{\mathbf{r}}_i - \hat{\mathbf{r}}_j - \mathbf{r}) | \Psi \rangle. \quad (4)$$

The two-body density $\rho^{(2)}(\mathbf{r})$ tells us about the probability to find a pair of nucleons at a given distance \mathbf{r} . In the case of ^{12}C where we expect an intrinsic α -cluster structure the two-body density should directly reflect the correlations between the α -clusters. The two-body density

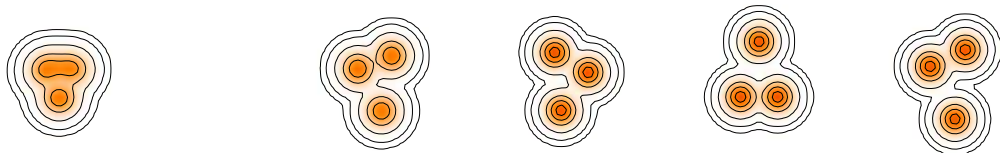


Figure 4. (Left) Intrinsic FMD basis state that has the largest overlap with the ground state. (Right) The four intrinsic FMD basis states that have the largest overlaps with the Hoyle state. The basis states are not orthogonal.

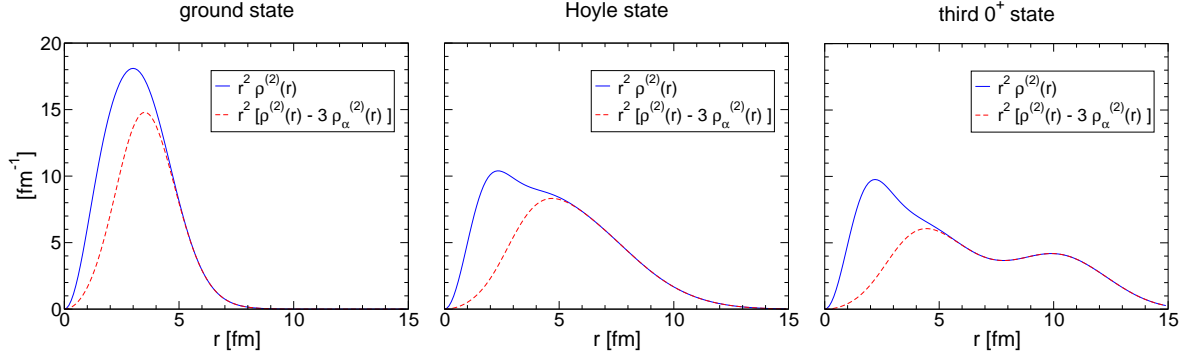


Figure 5. Two-body densities obtained in the cluster model for the ^{12}C ground state, the Hoyle state, and the third 0^+ state. The densities are multiplied by r^2 . Solid lines show the full two-body densities, the dashed lines show the results when the contributions to the two-body densities from inside the α -particles is subtracted.

is only smeared out by the finite size of the α -clusters. In microscopic many-body approaches the spin-isospin dependence of the two-body density could be used to validate the assumption of α -clustering. In principle the two-body densities will depend on the interaction used in the many-body approach. However this interaction dependence should only affect the behavior at very short distances. Here we are interested in the long-range correlations.

In the full two-body density also pairs of nucleons from the same α -particle are included. If we assume an α -cluster picture the more interesting observable is the probability to find a pair of nucleons from two different α -particles. In case of the cluster model one can simply subtract the contributions from within the α -particles. These are the dashed curves in Fig. 5. For the ground state the probability then peaks at about 3.5 fm reflecting the Pauli exclusion principle between the α clusters. For the Hoyle state we still find a single peak in the probability distribution at about 5 fm. This means that the α -particles in the Hoyle state are further apart from each other than in the ground state. The probability distribution also extends to much larger distances of more than 10 fm. The fact that there is only a single peak is consistent with the picture of a triangular structure where the distances between all three α -particles is the same. The density distributions of the third 0^+ state however shows a two-peak structure, with one peak at about 5 fm and another smaller peak at about 10 fm. This is what one would expect for a chain structure. The α -particles at the ends of the chain each see the α -particle in the middle of the chain at about 5 fm distance and the one at the other end of the chain at about 10 fm distance.

5.2. Expansion in oscillator basis

In no-core shell model calculations the second 0^+ state is found at much too high energies [17]. To illustrate the challenge for the no-core shell model we analyze the cluster model wave functions in the harmonic oscillator basis. Explicitly expanding our wave functions in the harmonic oscillator basis is not feasible. It is however easy to simply count the number of $N\hbar\Omega$ excitations in the wave function. This occupation probability can be calculated by

$$\text{Occ}(N) = \langle \Psi | \delta\left(\sum_i (\hat{H}_i^{HO}/\hbar\Omega - 3/2) - N\right) | \Psi \rangle \quad (5)$$

as proposed by Suzuki *et al.* [28]. The results are shown in Fig. 6 for the cluster model wave functions of the ground state and the Hoyle state. On the left an oscillator parameter $\hbar\Omega$ of 20 MeV was used. That corresponds roughly to the optimal oscillator parameter for the mean-field solution. In case of the ground state the contributions become very small for N larger

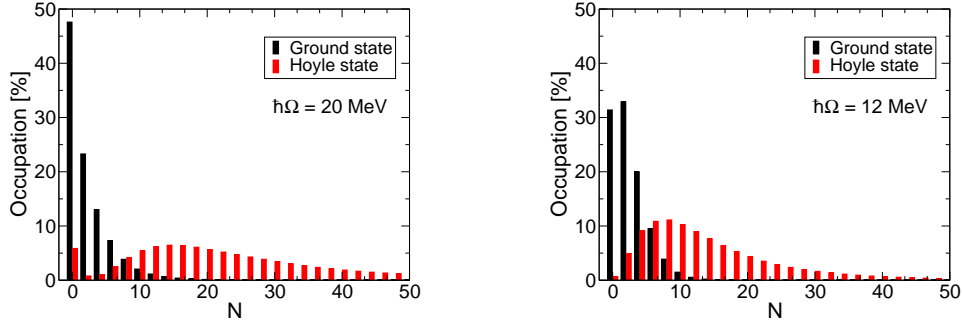


Figure 6. Decomposition of the ^{12}C ground state and the Hoyle state into $N\hbar\Omega$ components for oscillator constants of 20 MeV (left) and 12 MeV (right).

than 8 or 10. It is therefore not surprising that the NCSM calculations for the ground state can be converged. For the Hoyle state however, the distribution extends over a very large range of $N\hbar\Omega$. It is therefore clear that the Hoyle state can not be converged in NCSM calculations with $N_{\text{max}} = 8$ or even 10. The situation looks somewhat better for an oscillator parameter of 12 MeV as shown on the right hand side of Fig. 6. Here the distribution for the Hoyle state peaks at $N = 8$ and decays much more rapidly with N . However, standard NCSM calculations will not be able to reach large enough spaces. Maybe approaches like the importance truncated no-core shell model [29] or the symmetry adapted no-core shell model [30] will allow the description of the Hoyle state within the oscillator basis in the future.

References

- [1] Wiringa R B, Stoks V G J and Schiavilla R 1995 *Phys. Rev. C* **51** 38
- [2] Feldmeier H, Neff T, Roth R and Schnack J 1998 *Nucl. Phys.* **A632** 61
- [3] Neff T and Feldmeier H 2003 *Nucl. Phys.* **A713** 311
- [4] Roth R, Neff T and Feldmeier H 2010 *Prog. Part. Nucl. Phys.* **65** 50
- [5] Neff T 2011 *Phys. Rev. Lett.* **106** 042502
- [6] Adelberger E G *et al.* 1998 *Rev. Mod. Phys.* **70** 1265
- [7] Adelberger E G *et al.* 2011 *Rev. Mod. Phys.* **83** 195
- [8] Nara Singh B S, Hass M, Nir-El Y and Haquin G 2004 *Phys. Rev. Lett.* **93** 262503
- [9] Bemmerer D *et al.* 2006 *Phys. Rev. Lett.* **97** 122502
- [10] Confortola F *et al.* 2007 *Phys. Rev. C* **75** 065803
- [11] Brown T A D *et al.* 2007 *Phys. Rev. C* **76** 055801
- [12] Di Leva A *et al.* 2009 *Phys. Rev. Lett.* **102** 232502
- [13] Kim B T, Izumoto T and Nagatani K 1981 *Phys. Rev. C* **23** 33
- [14] Langanke K 1986 *Nucl. Phys.* **A457** 351
- [15] Kajino T 1986 *Nucl. Phys.* **A460** 559
- [16] Nollett K M 2001 *Phys. Rev.* **C63** 054002
- [17] Navrátil P, Gueorguiev V G, Vary J P, Ormand W E and Nogga A 2007 *Phys. Rev. Lett.* **99** 042501
- [18] Descouvemont P and Baye D 2010 *Rep. Prog. Phys.* **73** 036301
- [19] Nörtershäuser W *et al.* 2009 *Phys. Rev. Lett.* **102** 062503
- [20] Boykin W R, Baker S D and Hardy D M 1972 *Nucl. Phys.* **A195** 241
- [21] Spiger R J and Tombrello T A 1967 *Phys. Rev.* **163** 964
- [22] Brune C R, Kavanagh R W and Rolfs C 1994 *Phys. Rev. C* **50** 2205
- [23] Chernykh M, Feldmeier H, Neff T, von Neumann-Cosel P and Richter A 2007 *Phys. Rev. Lett.* **98** 032501
- [24] Kamimura M 1981 *Nucl. Phys.* **A351** 456
- [25] Funaki Y, Tohsaki A, Horiuchi H, Schuck P and Röpke G 2003 *Phys. Rev. C* **67** 051306(R)
- [26] Chernykh M, Feldmeier H, Neff T, von Neumann-Cosel P and Richter A 2010 *Phys. Rev. Lett.* **105** 022501
- [27] Epelbaum E, Krebs H, Lee D and Meißner U G 2011 *Phys. Rev. Lett.* **106** 192501
- [28] Suzuki Y, Arai K, Ogawa Y and Varga K 1996 *Phys. Rev. C* **54** 2073
- [29] Roth R and Navrátil P 2007 *Phys. Rev. Lett.* **99** 092501
- [30] Dytrych T, Sviratcheva K D, Bahri C, Draayer J P and Vary J P 2007 *Phys. Rev. Lett.* **98** 162503